An atomic force microscopy study of the effect of tensile loading and elevated temperature on polyvinylidene fluoride from flexible oil pipelines

D. GLENNON[1,2], J. R. SMITH[1], R. T. NEVELL[1], D. BEGG[2], S. E. MASON[3], K. L. WATSON[2], J. TSIBOUKLIS[1,*]
[1] *Division of Chemistry, Faculty of Science, University of Portsmouth, St. Michael's Building, White Swan Road, Portsmouth PO12DT, UK*
[2] *Department of Civil Engineering, Faculty of Environmental Studies, University of Portsmouth, Burnaby Building, Burnaby Road, Portsmouth, PO13QL, UK*
[3] *Department of Mechanical and Manufacturing Engineering, University of Portsmouth, Anglesea Building, Anglesea Road, Portsmouth PO13DJ, UK*

Flexible pipelines and risers have been used for more than 20 years for the transport of oil and gas in the petroleum industry. In the current study, a phase II polyvinylidene fluoride based pipeline material was subjected to varying degrees of tensile deformation, and microtomed sections were examined by atomic force microscopy (AFM) in order to investigate the resulting topographic changes. The effects of annealing at 100 and 130 °C on the maximum load and on topography were also studied. Annealing at 130 °C for varying lengths of time gave an increase in the maximum load which was found to be dependent upon crystallization kinetics. AFM studies showed ridges running perpendicular to the loading axis, which are attributed to flow lines resulting from the extrusion process. In annealed samples these ridges were closer together than in unannealed samples. The ridges were absent in quenched samples, but they gradually reappeared after storage at room temperature. These observations were further verified by transmission electron microscopy studies.

1. Introduction

Flexible oil pipelines are multilayered structures used for the transport of crude oil or natural gas from the seabed to the surface in offshore oil fields. There are two main types of flexible pipeline currently in service: bonded and unbonded. The former consist of elastomeric composite layers wrapped around and bounded to metallic sheaths. Unbonded pipelines consist of thermoplastic polymer layers separated by metallic cable wound or interlocked layers [1]. An inner polymer layer is provided to prevent leakage of the oil or gas. This layer must therefore be impermeable and oil-resistant. In order to prolong the service life of the pipe, the inner thermoplastic layer must also be resistant to other chemicals, such as volatile hydrocarbons and H_2S, which may be present in the oil. The outer thermoplastic layer provides insulation and corrosion protection for the steel layers. Consequently, the main design considerations in the choice of materials for this layer are impermeability to seawater and cost. The general criteria for choice of materials and design specifications for all layers appear to be: flexibility, elasticity, durability and strength [2].

Many published papers [1–3] in this field have examined the steel layers and their responses to corrosion and stress, but very few studies of the polymeric components have appeared in the literature. Dawans *et al.* [3] have attempted laboratory simulations of actual operating conditions and these were used for accelerated ageing tests to compare the ageing resistances of different inner sheath thermoplastics. The polymers investigated in these studies were high density polyethylene (HDPE), nylon 11, nylon 12 and polyvinylidene fluoride (PVDF). Nylon 11 was found to have adequate oil and gas resistance below 100 °C with a predicted lifetime of 10 years. PVDF was recommended for use at temperatures in the range of 100–130 °C, although no artificial ageing test results were given for this material [3].

A considerable number of papers have been published on the morphology and properties of PVDF since it was first commercially produced in 1968 [4–7]. Solid phase PVDF can exhibit three different spherulitic crystalline forms: phase I, phase II and phase III, depending upon the method of production. The degree of crystallinity of PVDF normally ranges

*Author for correspondence

0022–2461

from 35–65% [8]. The conformations of the polymer segments in these phases are *ttt*, *tgtg′* and *tgtg′ttt*, respectively, where *t* is *trans* ($\phi = 0°$), *g* is *gauche* ($\phi = 120°$) and *g′* is *gauche* minus ($\phi = -120°$). PVDF phases I and III are notable for their *pyro*- and *piezo*-electric properties although phase II shows little electrical activity. It is widely believed that the *tgtg′* conformation facilitates close packing of the chains by minimizing the non-bonded interactions of the fluorine atoms and that phase II is the lowest energy crystalline phase. All three phases have been studied in detail by X-ray diffraction (XRD) and by Fourier transform infra red (FTIR) and Raman spectroscopies. Comparisons have also been made between the spectra of crystalline samples and quenched samples. Significant differences in peak resonances for these three phases were observed. Phase II crystallinity in PVDF is exhibited in samples which have been allowed to solidify from the melt and the unit cell of the phase II crystal, elucidated from XRD studies [9], is a monoclinic system with two lattice points per unit mesh (Fig. 1).

Very few electron microscopy (EM) or atomic force microscopy (AFM) studies of PVDF have appeared in the literature. The majority of the few microscopy studies that do exist concentrate on supported monolayers of the polymer, with one recent exception in which scanning electron microscopy (SEM) was used to show that phase II PVDF can undergo a partial conversion to phases I and III on annealing [10].

In the current work, the semicrystalline morphology of the solid polymer has been imaged directly by AFM [11–13]. Crystallites in the samples under investigation were melt-grown under orientational stress due to the extrusion process. The effects of tensile deformation on the polymer were studied by varying the maximum extensions to which the samples had been subjected and then imaging the samples. Morphological changes which occurred on annealing were examined and compared with images from unannealed samples.

2. Experimental procedures

2.1. Materials

A sample of PVDF (melting range 157–220 °C, containing 10 wt% dibutyl sebacate plasticizer) was taken directly from the inner sheath of an unused commercial flexible oil pipe. The sheath was cut longitudinally into curved strips, which were machined flat and then into British Standard (BS 2782) [14] tensile testpieces with a length (l), width (w) and thickness (t) of 60 ± 0.5, 10 ± 0.5 and 3 ± 0.06 mm. After conditioning (application of tensile stress and/or annealing, as appropriate), small film sections were produced by microtoming from the relevant area of the testpiece (centre of sample, or necked/failed region after stretching).

2.2. Instrumentation

Tensile measurements were obtained using a Lloyd SR 100 instrument fitted with a 30 kN load cell. The internal extensometer was used and data were plotted as force versus extension curves. AFM studies were performed in air under ambient conditions using a Discoverer TopoMetrix TMX2000 Scanning Probe Microscope (SPM) instrument (TopoMetrix Corporation, Saffron Waldon, Essex, UK). Transmission electron microscopy (TEM) studies were performed using a Philips EM300 electron microscope.

2.3. Methods

The testpieces were divided into groups of eight samples and each group was subjected to predetermined annealing conditions, (i) at 100 °C and (ii) at 130 °C. The strained samples were given numbers according to their positions along the force versus extension curves, as shown in Fig. 2. Preconditioning and strain regimes of all samples are listed in Table I.

A film sample of PVDF taken from an unstretched, unannealed sample (group **a**) was heated to 160 °C, i.e., just into the melting range, and quenched with liquid nitrogen in order to inhibit crystallization. This

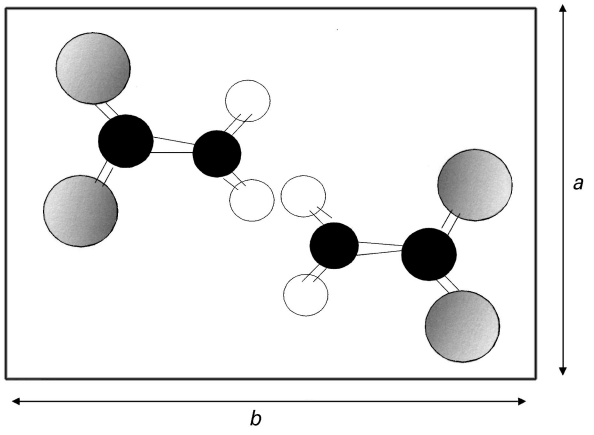

Figure 1 A plan view of unit cell of phase II PVDF projected on the (001) plane. Carbon atoms are shown in black, fluorine atoms are shown in grey and hydrogens are shown in white.

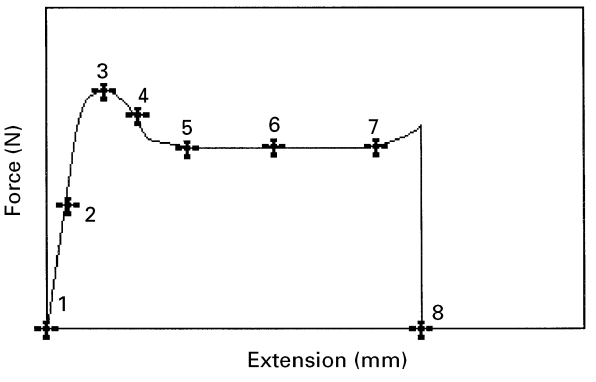

Figure 2 A schematic diagram indicating the tensile extension regimes to which the samples have been exposed. Sample 1 = unstrained, sample 2 = elastic region, sample 3 = onset of necking, sample 4 = neck development, sample 5 = neck stabilization, sample 6 = mid neck region, sample 7 = end of neck region and sample 8 = failure.

TABLE I The preconditioning and strain regimes of all samples

Numeral	Group name	Sample number	Annealing conditions	Strain regime
None				
	a	1	Unannealed	Unstrained
		2		Elastic region
		3		Onset of necking
		4		Neck development
		5		Neck stabilization
		6		Neck growth
		7		End of necking
		8		Failure
i				
	b		100 °C for 3 h	
	c	As for group **a**	100 °C for 24 h	As for group **a**
	d		100 °C for 1 week	
ii				
	b		130 °C for 3 h	
	c		130 °C for 24 h	
	d	As for group **a**	130 °C for 1 week	As for group **a**
	e		130 °C for 1 month.	

sample was then examined by AFM as before. A test-piece was cut from the quenched material and the width and thickness were found to be uniform along the straight section ($l = 60 \pm 0.5$ mm, $w = 11 \pm 0.5$ mm, $t = 1.6 \pm 0.05$ mm).

All samples were strained at 10 mm min^{-1}. After the appropriate conditioning described above, small film sections of the polymer were prepared from each specimen by microtoming along the loading axis from the relevant regions of the test-pieces. Selected film specimens were then imaged by SPM and TEM.

2.4. Atomic force microscopy (AFM) studies

A scanner capable of a maximum X–Y translation of 70×70 μm was used and imaging was performed in contact mode using standard profile silicon nitride tips mounted on cantilevers of force constant 0.036 N m^{-1}. Graphical output was displayed on a monitor with a resolution of 500 lines × 500 pixels. Images were levelled by plane-fitting but no other image processing was carried out. Roughness average values, R_a, were calculated for unannealed and quenched samples using TopoMetrix image analysis software [15]; R_a is defined as the arithmetic average of the absolute values of the measured profile height deviations given by Equation 1.

$$R_a = \frac{1}{n} \sum_{i=1}^{n} |Z_i - \bar{Z}| \quad (1)$$

where, n is the number of height positions along line profile; Z_i is the height at position i (nm) and $\bar{Z}$ is the average height (nm).

In these studies, values of R_a were obtained from 5 μm line sections of the image. The procedure was repeated 25 times per sample and the mean-average and standard deviations calculated.

3. Results and discussion

3.1. Mechanical testing

Force versus extension curves for unannealed samples (group **a**) and those annealed for 1 week at 100 °C (group i **d**) and 130 °C (group ii **d**) are shown in Fig. 3(a–c). Sample numbers are marked at their points of maximum extension. It can be seen that after annealing, the force versus extension curves are less reproducible than similar plots obtained from unannealed samples (group **a**). This reduction is evidenced as a scattering of the data, with plastic transitions and failures occurring at different extension values.

Fig. 3(d and e) are overlaid force versus extension curves for all the samples strained to failure for both groups (i **a**–**d** and ii **a**–**e**). The following trends are observed with increased exposure time of the polymer to higher temperatures: (i) the maximum load increases; (ii) the onset of neck stabilization moves towards lower extension values; and (iii) the failure behaviour of the annealed material becomes more susceptible to surface flaws.

The onset of neck stabilization is evidenced from the force versus extension plots as a stationary point just before the plateau, point 5 in Figs 2 and 3(a–e). After the plateau, a second stationary point is observed prior to failure. As the failure behaviour becomes more susceptible to flaws, extension at break becomes less predictable and some samples fail before the onset of necking. Two possible explanations for this phenomenon are the volatilization of the plasticizer and partial degradation of the polymer.

Fig. 4 shows the effect of increasing the annealing temperature. The samples plotted are (a) samples **a**8, (b) sample i **d**8 and (c) sample ii **d**8. It appears that annealing at 100 °C gives rise to a higher maximum load, greater extension and better reproducibility of force versus extension data than annealing at 130 °C.

A force versus extension plot for a quenched tensile test-piece was also obtained (Fig. 5). Exact stress and

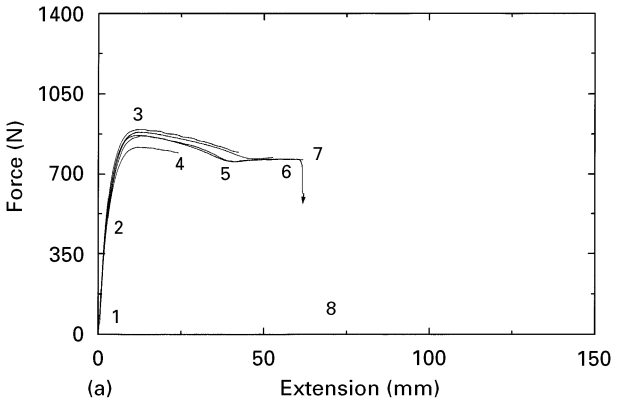

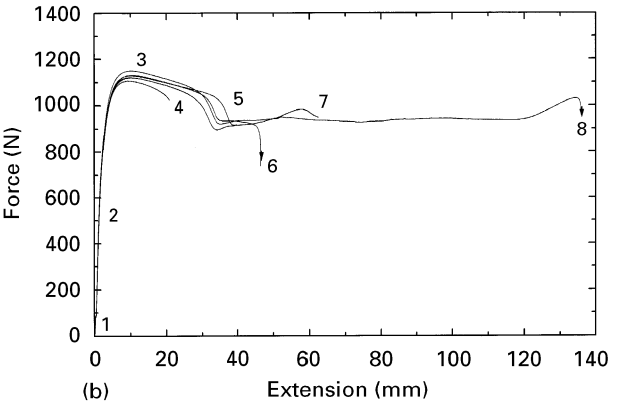

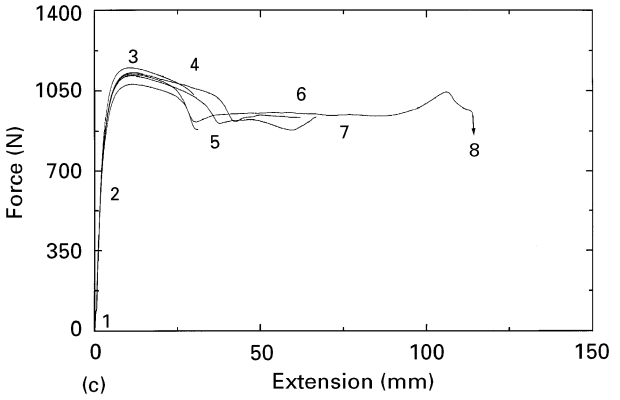

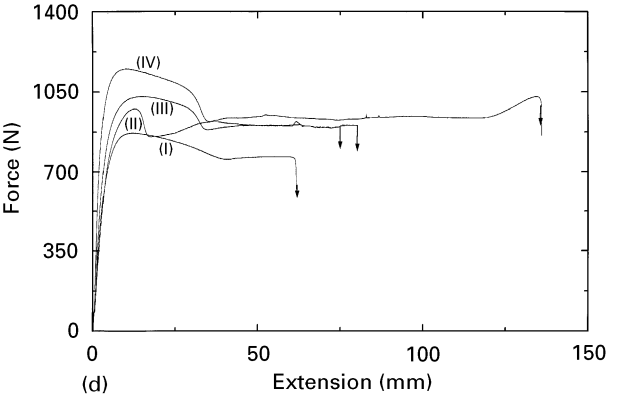

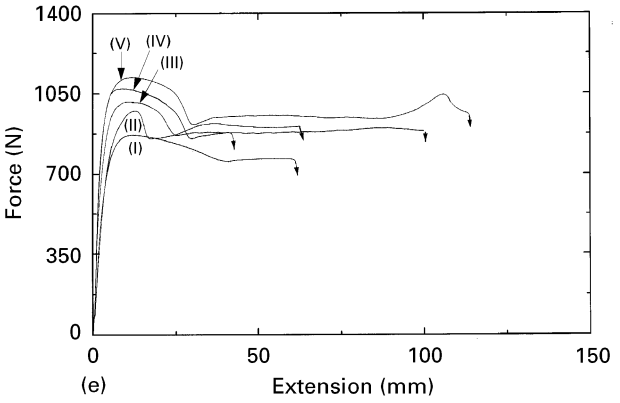

Figure 3 Force versus extension curves of (a) all group **a** samples, (b) all group i **d** samples (c) all group ii **d** samples (d) samples (i) **a**8, (ii) i **b**8, (iii) i **d**8 and (iv) i **d**8 and (e) samples (i) **a**8, (ii) i **b**8, (iii) ii **c**8, (iv) ii **d**8 and (v) ii **e**8.

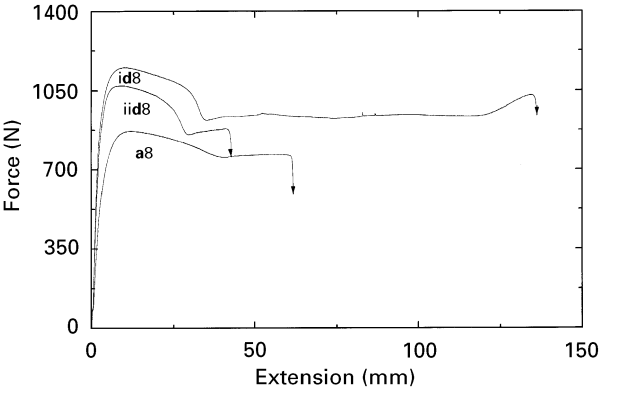

Figure 4 Force versus extension curves showing the differences between unannealed samples (**a**8) samples annealed at 100 °C (i **d**8) and samples annealed at 130 °C (ii **d**8).

strain values were not calculated as an internal extensometer was used for these experiments; approximate stress and strain values indicate that the maximum stress acting on the quenched test-piece was lower than the maximum stress acting on any of the other samples (less than half of the maximum stress obtained for samples annealed for 1 week (group **d**)) and the maximum strain was approximately equal to the maximum strain obtained for unannealed samples (group **a**).

The quenched sample became opaque after the elastic–plastic transition region of the force versus extension curve and remained opaque until failure; at this point the necked region became transparent. This may indicate a reversion to the amorphous state in this region. Approximate stresses of unannealed samples (group **a**) and those which had been annealed for 1 week at 130 °C (group ii **d**), and the quenched sample are given in Table II.

The rate of secondary crystal growth in polymers is governed by the *Avrami equation* [16]:

$$\varphi = \varphi_\infty[1 - \exp(-zt^n)] \quad (2)$$

where, φ is the volume fraction crystallinity; φ_∞ is the volume fraction crystallinity after an infinite length of time; t is the time; n is the Avrami exponent, and z is a constant.

The average maximum force (calculated as the mean maximum load from six sets of force versus extension data) for each group of samples annealed at 130 °C is plotted as a function of annealing time and

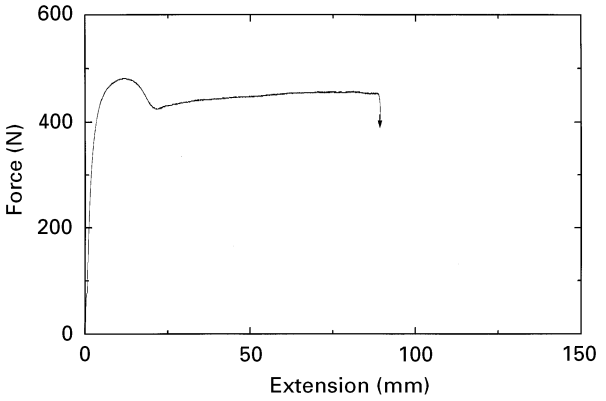

Figure 5 Force versus extension curve obtained from the quenched PVDF sample.

a fit of $y = 1125(1 - e^{-(x+1)^4})$ is included (Fig. 6a). Similarities between the average maximum force plot and the approximate Avrami fit leads to the conclusion that the increase in average maximum load, F_{max}, on annealing is due to increased crystallinity. The increase in maximum load on the polymer due to increasing annealing time is given by:

$$F_{max} = F_{max,\infty}(1 - e^{-z'(t+1)^{n'}}) \quad (3)$$

Where $F_{max,\infty}$ is the average maximum load after annealing for an infinite time, and n' and z' are the maximum force versus time equation equivalents of the Avrami constants. The $(t + 1)$ term is used instead of t because at $t = 0$ in the Avrami equation, the polymer is assumed to be entirely amorphous, usually

TABLE II The approximate stress, strain and tensile modulus values of PVDF from groups **a** and ii **d** and the quenched sample at maximum load. The approximate breaking strain of the quenched sample is also shown.

Sample	Cross-sectional area (mm^2)	F_{max} (N)[a]	e_{max} (mm)[b]	Stress, σ (MPa)	Strain, ε	Modulus, E (MPa)	Strain at break
Group **a**							
1	29.52	0.00	0.00	0	0.00	n/a	
2	28.32	484.80	2.51	17	0.04	n/a	
3	29.85	884.50	11.66	29	0.19	152	
4	29.74	818.20	11.49	28	0.19	144	
5	29.51	896.10	11.75	30	0.20	155	
6	29.69	884.40	12.84	30	0.21	139	
7	29.97	867.80	12.70	29	0.21	137	
8	29.80	870.50	11.28	29	0.19	155	
Group (ii) **d**							
1	28.43	0.00	0.00	0	0.00	n/a	
2	28.02	676.00	1.92	24	0.03	n/a	
3	28.52	1132.00	11.01	40	0.18	216	
4	28.23	1152.00	9.89	41	0.16	248	
5	27.72	1080.00	10.95	39	0.18	213	
6	28.73	1125.00	10.62	39	0.18	221	
7	28.45	1117.00	11.48	39	0.19	205	
8	28.19	1121.00	11.18	40	0.19	213	
Quenched **q**1	23.50	481.70	11.08	21	0.18	111	1.49

[a] F_{max} = maximum load,
[b] e_{max} = extension at maximum load

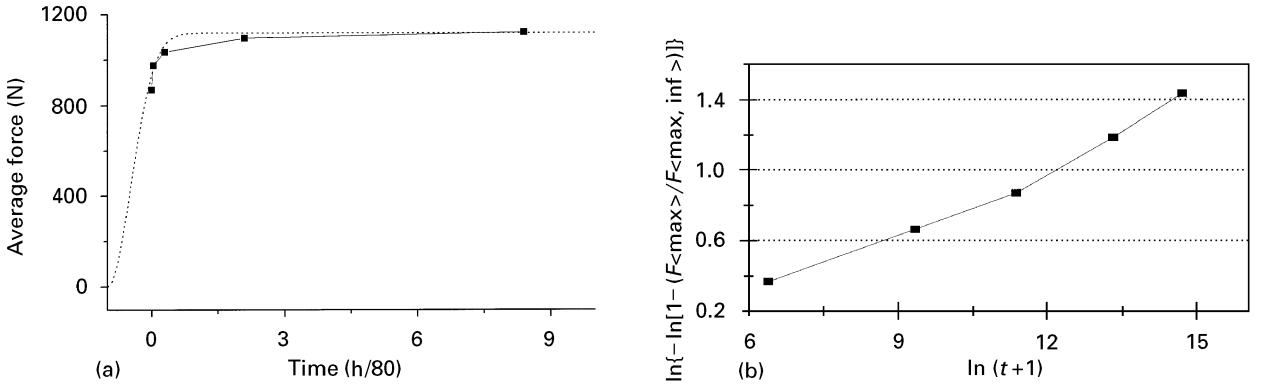

Figure 6 (a) A plot of average maximum force *vs.* annealing time for PVDF samples annealed at 130 °C. Each data point represents the average of six samples. The dotted line is a plot of $y = 1125\ (1 - e^{-(x+1)^4})$ and (b) a plot of $\ln[-\ln(1 - F/F_\infty)]$ versus $\ln\ (t + 1)$ where $F_\infty = 1139$N.

in solution or melt form. In the current work, the samples had already undergone solidification and crystallization after processing and the $(t + 1)$ factor allows 1 h for this process. A 1 h cooling time was chosen arbitrarily to correspond with the assumption that the increase in maximum force is entirely due to secondary crystallization on annealing.

The value of F_∞ was obtained by a least squares linear regression method using:

$$\ln[-\ln(1 - F_{max}/F_{max,\infty})] = \ln z' + n' \ln(t + 1) \quad (4)$$

The linear regression method was applied to a plot of $\ln[-\ln(1 - F_{max}/F_{max,\infty})]$ versus $\ln(t + c)$ where $c = 10$ min (Fig. 6b). This analysis yielded $F_\infty = 1139$ N in PVDF samples annealed at 130 °C, with an error value of $R^2 = 0.98$.

3.2. AFM studies

3.2.1. Topography of unannealed PVDF

AFM images (Fig. 7(a–f)) of the unannealed samples revealed ridged surface structures running perpendicular to the loading axis (the long axis of the tensile test-piece). These ridges are attributed to flow lines resulting from the extrusion process. As the extension increased, thin voids appeared in the structure and these were oriented approximately parallel to the loading axis. The ridged structure was still observable but became less uniform and started to bend in the direction of the loading axis, giving rise to small hollows.

3.2.2. Effect of annealing

Similar ridged structures, showing thin voids running along the loading axis were also observed in the AFM images of the 130 °C annealed samples (group ii **d**) (Fig. 8(a–c)). The ridges also appeared to be closer together than in the unannealed samples and this may be attributed to shrinkage of the polymer due to increased crystallinity. Shrinkage arises because the crystalline material is more dense than the amorphous polymer. The thin voids running parallel to the loading axis were less evident in the annealed samples. After stretching the polymer, the average distance between ridges appeared to decrease in the annealed samples. This may have been due to further crystallization induced by the strain hardening process.

A transmission electron micrograph (TEM) of a sample annealed at 130 °C for 24 h at the point of fracture (point 8 of group ii **c**) is shown in Fig. 9a. The ridges can be seen running perpendicular to the loading axis and some of these ridges are broken up, curving in the direction of the loading axis. A TEM at higher magnification also reveals possible voids aligned in the loading axis (Fig. 9b).

3.2.3. Effect of quenching

Initial imaging of the surface, shortly after quenching, revealed a much smoother topography than for both annealed and unannealed samples (Fig. 10a). Statistical measurements showed that the material possessed an arithmetic surface roughness average of 31 ± 13 nm

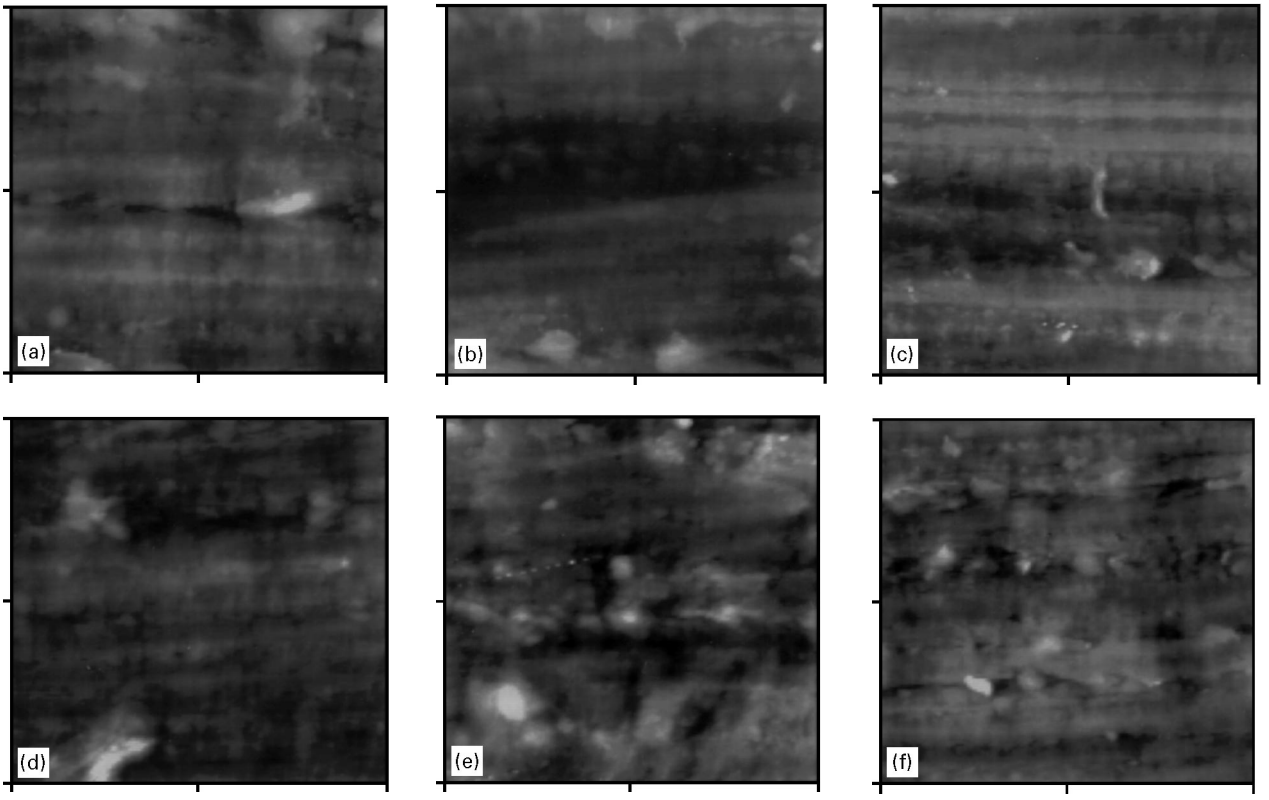

Figure 7 AFM micrographs of unannealed samples obtained in contact mode. The loading axis runs from top to bottom in all cases. Dimensions $x = y = 60$ μm. (a) sample **a**1, (b) sample **a**3, (c) sample **a**4, (d) sample **a**6, (e) sample **a**7, and (f) sample **a**8.

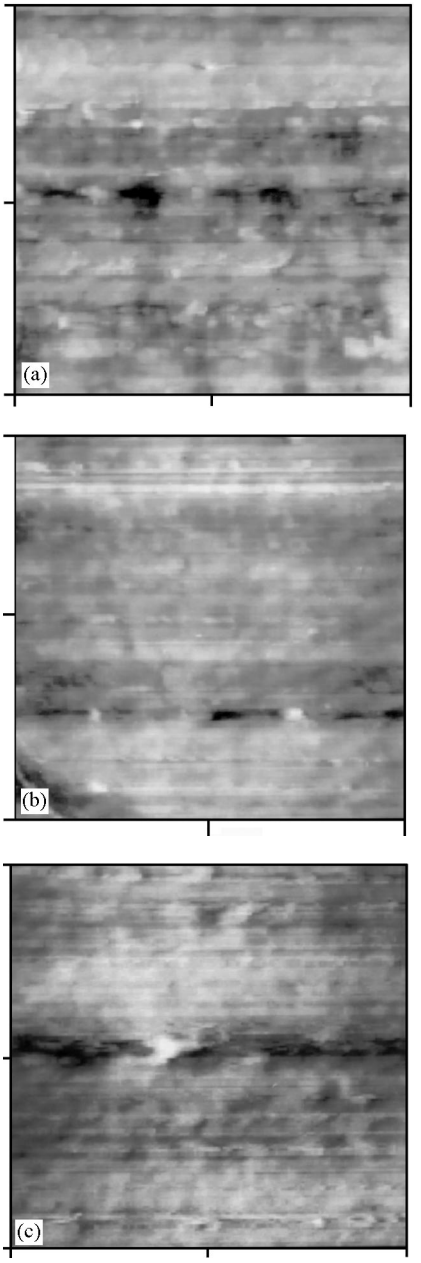

Figure 8 AFM micrographs of annealed PVDF samples obtained in contact mode. Dimensions: $x = y = 55\ \mu m$ in all cases (a) ii **d**1 (unstretched), (b) ii **d**3 (maximum load) and (c) ii **d**7 (end of necked region prior to failure. The loading axis is parallel to the length of the paper in all cases.

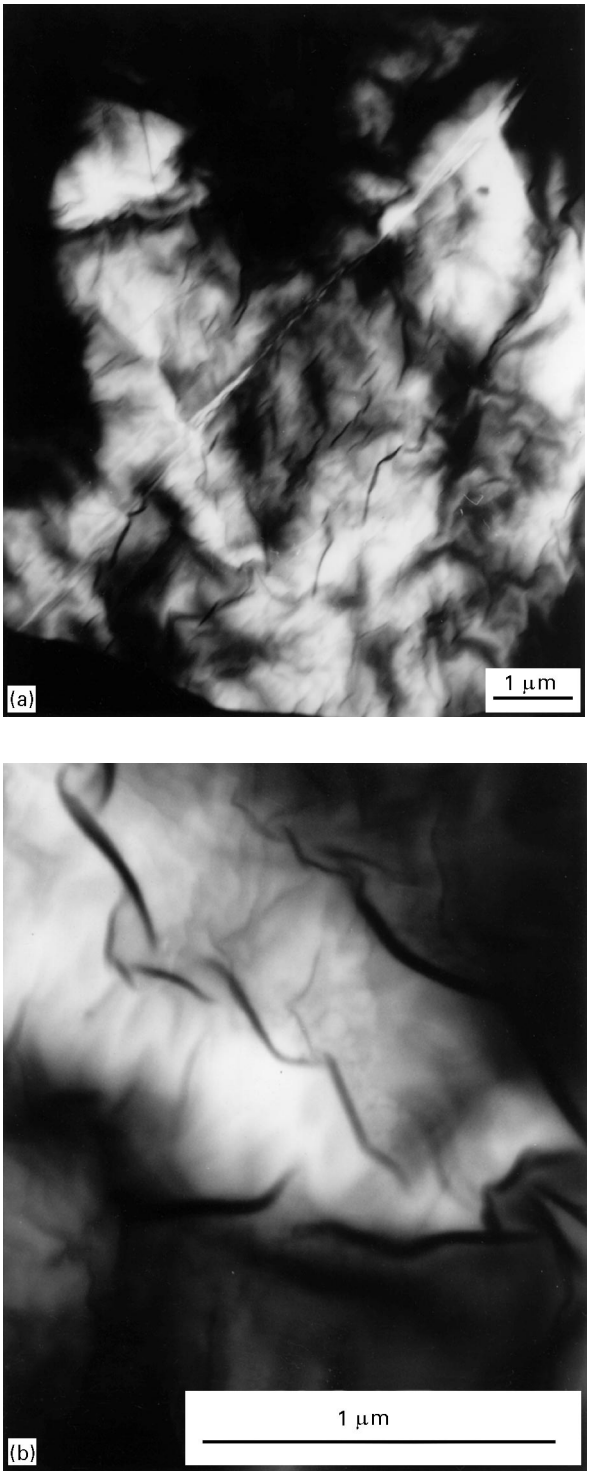

Figure 9 TEM micrographs of PVDF sample ii **c**8: (a) a low magnification micrograph showing the ridges running perpendicular to the loading axis, and (b) at higher magnification showing the presence of possible ridges (indicated by arrows).

compared with 66 ± 44 nm for the unstressed, unannealed sample. After a 6 week period of storage at room temperature, the ridges that were present in the original, unannealed sample began to reappear in the quenched sample (Fig. 10b). The re-emergence of ridges due to storage at a temperature above the glass transition temperature, T_g, of the material may be an effect of "elastic memory", i.e., the ridges are areas of localized, "moulded-in" stress.

4. Conclusions

The tensile strength of the PVDF used in this study increases on annealing at either 100 or 130 °C. The samples annealed at 130 °C demonstrate a more erratic failure behaviour and greater susceptibility to surface flaws than those annealed at 100 °C. Two possible explanations for the reduction in maximum extension of some of the samples annealed at 130 °C may be the volatilization of the plasticizer or partial degradation of the polymer. AFM studies of these samples gave no indication of degradation. A quenched sample showed a lower maximum stress and greater ductility than the other samples investigated.

A plot of average maximum force (each data point averaged over six samples) versus annealing time was

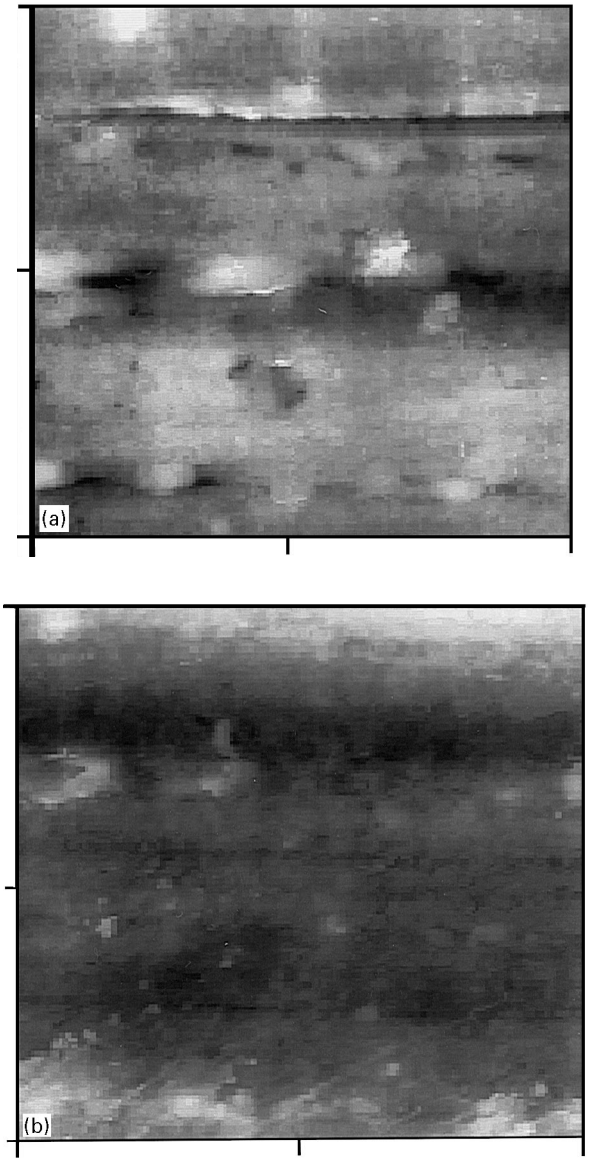

Figure 10 AFM micrographs of quenched PVDF sample. Dimensions: $x = y = 60$ μm (a) is an initial scan and (b) is a scan of the sample after 6 weeks of storage at room temperature.

recorded. The plot appeared to show an Avrami relationship between maximum load and annealing time, indicating that the increase in maximum load due to annealing of PVDF is a function of the degree of crystallinity of the polymer.

AFM studies of the unannealed polymer showed signs of orientation, evidenced as flow lines, due to the manufacturing process. As the tensile deformation of the samples increased, the material showed signs of stress induced orientation and a breakdown of the flow lines by the formation of cracks along the tensile axis. The quenched sample showed no evidence of flow lines initially, although these did re-emerge after six weeks of storage at room temperature (above the T_g of PVDF). AFM imaging of annealed samples also revealed a similar ridged structure to the unannealed samples, but with reduced spacing between ridges. This last effect may be caused by shrinkage of the polymer due to increased crystallinity. TEM confirmed the presence of the ridges and thin voids parallel to the load axis in the tensile stressed samples.

Acknowledgements

DG and JRS wish to thank the University of Portsmouth for the awards of a research bursary and a postdoctoral research fellowship, respectively.

References

1. Ø. BALTZERSEN and T. I. WAAG, *NDT & E Int.* **26** (1993) 241.
2. F. MOORE, *Engng. Struct.* **11** (1989) 208.
3. F. DAWANS, J. JARRIN and J. HARDY, *SPE Production Engng.* (1988) 387.
4. K. NAKAGAWA and Y. ISHIDA, *J. Polym. Sci., Polym. Phys. Ed.* **11** (1973) 1503.
5. M. A. BACHMANN, W. L. GORDON, J. L. KOENIG and J. B. LANDO, *J. Appl. Phys.* **50** (1979) 6106.
6. M. KOBAYASHI, K. TASHIRO and T. HIROYUKI, *Macromolecules* **8** (1975) 158.
7. W. M. PREST, Jr. and D. J. LUCA, *J. Appl. Phys.* **46** (1975) 4136.
8. J. E. DOHANY and L. E. ROBB, in "Kirk–Othmer encyclopaedia of chemical technology", Vol. 11, 3rd Edn. edited by D. F. Othmer, (Wiley Interscience, New York, 1980).
9. R. HASEGAWA, Y. TAKAHASHI, Y. CHATANI and H. TADOKORO, *Polym. J.* **3** (1972) 600.
10. G. LAROCHE, Y. MAROIS, R. GUIDOIN, M. W. KING, L. MARTIN, T. HOW and Y. DOUVILLE, *J. Biomed. Mater. Res.* **29** (1995) 1525.
11. G. BINNIG, C. F. QUATE and Ch. GERBER, *Phys. Rev. Lett.* **56** (1986) 930.
12. C. M. MATE, G. M. McCLELLAND, R. ERLANDSON and S. CHIANG, *Phys. Rev. Lett.* **59** (1987) 1742.
13. N. A. BURNHAM and R. J. COLTON, in "Scanning tunnelling microscopy and spectroscopy", edited by D. A. Bonnell, (VCH Press, New York, 1993).
14. BS 2782: Part 3: Methods 320A to 320F. Tensile Strength, Elongation and Elastic Modulus, Method 320A, BSI 1976.
15. SPM Laboratory, Image Analysis Software, Version 3.06, TopoMetrix Corporation, Santa Clara, CA, USA.
16. H.-G. ELIAS, in "Macromolecules, Vol. 1 structure and properties", edited by J. W. Stafford, (John Wiley, New York, 1977).

Received 25 October 1996
and accepted 1 May 1997